JOURNAL OF AIRCRAFT
Vol. 38, No. 4, July–August 2001

Hypersonic Drag and Heat-Transfer Reduction Using a Forward-Facing Jet

Benjamin Meyer,* H. F. Nelson,† and David W. Riggins‡
University of Missouri—Rolla, Rolla, Missouri 65409-0050

A two-dimensional numerical study of the effects of a forward-facing jet located at the stagnation point of a blunt body on wave drag, heat transfer, and skin-friction drag is presented for Mach 6.5 flow at 30 km altitude. The full Navier–Stokes equations are used with variable viscosity and thermal conductivity. It is shown that upstream injection can significantly modify the flowfield. If the jet conditions are chosen properly, large reductions in drag and heat transfer can be obtained resulting in possible increases in the volumetric efficiency and static stability of aircraft as well as reductions in the heating protection requirements for hypersonic vehicles.

Nomenclature

A_e	=	jet exit area per unit width, m^2/m
C_T	=	jet thrust coefficient
D	=	wave drag per unit width, N/m
d/d_j	=	body diameter to jet diameter ratio
d_j	=	jet diameter, m
F	=	skin-friction drag per unit width, N/m
F_N	=	nose skin-friction drag per unit width, N/m
M_j	=	jet exit Mach number
M_∞	=	freestream Mach, 6.5
$\dot{m}$	=	mass-flow rate, kg/s
P	=	pressure, Pa
P/P_{t2}	=	ratio of pressure to no injection total pressure after main normal shock
P_{tj}	=	jet total pressure, 375 kPa
$P_{t\infty}$	=	freestream total pressure
P_∞	=	freestream pressure, 1185.5 Pa
Q	=	heat-transfer rate per unit width, W/m
q	=	dynamic pressure, Pa
R_D	=	wave drag ratio, D/D_{ref}
R_F	=	skin-friction drag ratio, F/F_{ref}
R_Q	=	heat-transfer ratio, Q/Q_{ref}
R_Δ	=	shock stand-off ratio, $\Delta/\Delta_{\text{ref}}$
r	=	body nose radius, m
T_j	=	jet thrust per unit width, N/m
T_∞	=	freestream temperature, 231.24 K
V_e	=	jet exit velocity, m/s
Δ	=	shock stand-off distance, m
θ	=	angle on body, deg

Introduction

TWO major problems in hypersonic flight are large wave drag and surface heating. Both problems can be alleviated by modifying the flowfield in front of the body. It is well known that using a structural spike extending from the nose of a blunt body flying at supersonic speeds can significantly reduce drag.[1] A spike has also been shown to reduce the heat transfer to the body surface.[2] However, the spike becomes hot and ablates as a result of large stagnation temperatures, hence requiring frequent replacement or active cooling. It has been suggested that depositing energy upstream can reduce drag of blunt bodies, e.g., the drag of a cylinder wedge was reduced by up to 70% using energy deposition.[3] However, deposition of energy upstream, in whatever manner accomplished, generally results in increased heat transfer to the surface of the body. Riggins et al.[3] stated that there is approximately a 30% increase in heat transfer associated with a 50% drop in external drag using upstream energy deposition. An experimental investigation, which employed both a physical spike and energy deposition at the tip of the spike, was done by Toro et al.[4] Several cases were studied: 1) blunt body without a spike, 2) spiked blunt body without tip cooling gas and no energy injection, 3) spiked blunt body with sonic cooling gas from tip and no energy injection, and 4) spiked blunt body with cooling gas and energy injection. It was found that the wave drag decreased sequentially from case 1 to case 4. In a similar study it was also found that the heat transfer of case 3 was smaller than that of the original blunt body without a spike.[5]

A more desirable method to reduce drag and heat transfer may be to deposit energy in front of the body without using a physical spike. One method for depositing energy upstream of the body is to inject a combustible mixture, such as a hydrogen-air mixture, from the nose of the body and take advantage of a shock-induced combustion reaction. This will result in a large upstream energy release. However, Matsuo et al.[6] showed that upstream combustion results in a large temperature increase along the stagnation streamline behind the bow shock. This inevitably increases heat transfer to the body. However, the use of a noncombustible fluid jet, such as an air jet, will produce a pressure variation on the forebody similar to that observed with a spike,[7] without the heating/structural issues generated by a spike. This paper focuses on the use of inert forward-facing jets for obtaining overall drag and heat-transfer reductions on blunt-body leading edges at hypersonic velocities.

Charczenko and Hennessey[7] observed a noticeable decrease in pressure on the nose of a blunt body caused by upstream-directed jet thrust. They found that for constant jet thrust the pressure decreases further as the freestream Mach number increases. This means that for constant jet thrust one expects to see more favorable drag reduction as freestream Mach number is increased. In fact, a study done by Love[8] at a freestream Mach number of 1.62 showed that, at this low Mach number, the savings in drag by using a forward-facing jet to change the shock layer structure may not be as beneficial as simply placing the jet at the aft of the body because the thrust of the jet exceeds any observed reduction in drag.

A broad investigation by Romeo and Sterrett[9] found that there are two distinct ways that an upstream-directed jet can affect a blunt-body shock. First, at small $P_{\text{tj}}/P_{t\infty}$ the shock is pushed away from the body and does not significantly change in shape. The shock is similar to that which occurs if the blunt body is increased in size. Second, at large ratios of $P_{\text{tj}}/P_{t\infty}$ the shock stand-off distance

Received 13 March 2000; revision received 10 December 2000; accepted for publication 15 December 2000.

*Graduate Research Assistant; currently Research Engineer, Swales Aerospace, Hampton, VA 23681. Student Member AIAA.

†Professor of Aerospace Engineering, Thermal Radiative Transfer Group, Department of Mechanical and Aerospace Engineering and Engineering Mechanics. Associate Fellow AIAA.

‡Professor of Aerospace Engineering, Department of Mechanical and Aerospace Engineering and Engineering Mechanics. Senior Member AIAA.

becomes very large, the jet resembles a spike, and the shock shape changes to resemble that of flow over a body with a sharp leading edge (an oblique shock system forms). The spike is unstable in this second type of flow. These two flow types were also found by Tolle,[10] who conducted a study at Mach 14. He found that when the ratio of jet momentum to freestream momentum became greater than 0.1 the flow changed from blunt-body flow to spike flow for bodies at zero angle of attack.

The instability of the spike flow exhibits two different forms.[9,10] The first is a lateral movement in which the shock stays in approximately the same axial location. The second is a cyclic collapse to a blunt-body shock. Tolle explains that the collapse is caused by the reduced "rigidity" of the longer aerodynamic spike. Small pressure fluctuations on the sides of the aerodynamic spike cause it to move off the axis of symmetry. This, in turn, shortens the spike, and the shock moves closer to the body. Because the spike is now shorter, it centers itself fairly easily, and the length of the spike begins to increase, starting the cycle again.

In general, the larger jet thrust required to produce such "spike" flow results in net increases to the overall drag making the jet counterproductive. Consequently, this study focuses on the blunt-body-type flow. Specifically, the effects on blunt-body overall wave drag, heat transfer, and skin-friction drag caused by a forward-facing jet are examined by parametrically varying jet exit diameter and exit Mach number while maintaining constant injectant reservoir pressure and temperature.

Computational Methodology

This analysis was done using a modified two-dimensional version of the time-marching Navier–Stokes code SPARK, which was developed at NASA Langley Research Center by Drummond et al.[11] The full laminar Navier–Stokes equations with variable thermodynamic and diffusion properties as well as variable specific heats are solved in an explicit time-marching fashion. The code has the capability to model combustion; however, air was used for injection in this study. Dissociation effects were not considered. All calculations used a constant Prandtl number of 0.7. All cases were run at zero angle of attack and were forced to be symmetrical by imposing symmetry conditions along the stagnation streamline of the body. Thus stability issues of the jet are not investigated. For the no-injection and injection cases 236×157 (angular by radial) and 145×97 body-fitted grids clustered at the body surface were used, respectively. The inflow boundary conditions used standard values for an altitude of 30 km: $P_\infty = 1185.5$ Pa and $T_\infty = 231.24$ K. The outflow boundaries used simple extrapolation for all variables. Viscous (no slip) conditions were taken everywhere on the body. Pressure on the body was extrapolated at the local normal. The body surface was maintained at 500 K. Convergence to steady state was based on the achievement of asymptotic values for wave drag, heat transfer, and skin-friction drag. For the injection cases a steady-state solution was obtained at approximately 225,000 iterations; however, all cases were run an additional 75,000 iterations to ensure time convergence. Grid- and time-convergence issues are addressed in Appendix A.

Analysis

Two of the important variables for drag studies with upstream injection are shock stand-off distance Δ and body diameter to jet diameter ratio d/d_j. To compare results to the reference (no injection) results, a ratio R_i is defined, where i represents variables such as shock stand-off distance, wave drag, heat transfer, and skin-friction drag. R_i is defined as the ratio of a variable to the same variable for the reference (no injection) case (e.g., in the case of wave drag: $R_D = D/D_{\text{ref}}$). For the case of wave drag, the thrust penalty of the forward-facing jet is included in the overall wave drag value D. The smaller the value of R_i the more beneficial the reduction in the variable. When $R_i = 1$, the variable has the same value as that of the no-injection case. In the case of R_Q, negative values indicate that the body is being cooled (losing heat). Thus, if the no-injection case has a heating rate of 100 W/m and a given injection case has a value $R_Q = -1$, then the body is cooling at a rate of 100 W/m.

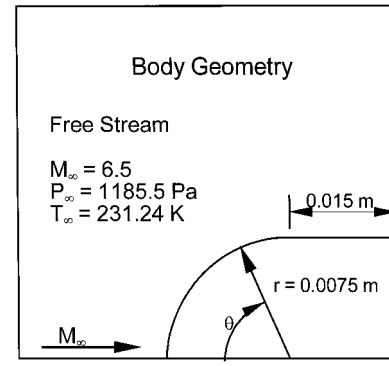

Fig. 1 Body geometry and inlet conditions (half-body shown).

For this analysis the thrust for the forward-facing jet is defined as

$$T_j = \dot{m} V_e + A_e P_e \tag{1}$$

The thrust coefficient is defined as

$$C_T = T_j / q_\infty A \tag{2}$$

where A is defined as the maximum cross-sectional area of the blunt body. It is important to keep in mind throughout this analysis that the jet total pressure and temperature are constant. Thus, for a given exit area, an increase in jet exit Mach number results in a decrease in thrust (see Appendix B).

Geometry

Figure 1 shows the blunt body used in this research. The nose radius is 0.0075 m. The analysis is two-dimensional; hence, parameters such as drag are per meter width. The geometry corresponds to the leading edge of a wing. The length of the body in the flow direction, not including the nose, is 0.015 m. Although this length has no bearing on wave-drag calculations (the angle of attack is always zero), it is included in heat transfer and skin-friction drag integrations over the surface. The sides of the body are important because if a reattachment shock is present its effects are not necessarily restricted to the nose region defined by $0 \le \theta \le 90$ deg. The sides of the body can experience varying temperatures and velocities and thus become important for a complete analysis. The jet is centered at the nose of the body ($\theta = 0$, $r = 0.0075$ m) and faces into the freestream. The angle of attack of the body and the jet are fixed at zero.

Comparison to Previous Work

Finley[12] published experimental work in which a jet was injected upstream into Mach 2.5 flow. His investigation covered a range of shapes, d/d_j ratios, and ratios of total jet pressure to after shock total pressure P_{tj}/P_{t2}. He found that three regimes existed as a function of P_{tj}/P_{t2}. Regime 1, P_{tj}/P_{t2} increasing from 1, was a steady flow with multiple jet cells. As P_{tj}/P_{t2} increased further, there was a small range of P_{tj}/P_{t2} where the flow became unsteady as a result of the multiple jet cells. Finley calls this range regime 2. Regime 2 ends when a critical ratio of P_{tj}/P_{t2} is reached. For ratios larger than the critical, regime 3, one jet cell existed, and the flow was stable.

To verify the computational analysis, one of Finley's cases was run. The same computational setup for injection previously mentioned was used, except the incoming conditions were changed to those used by Finley and the body temperature was held at 300 K. Incoming conditions were as follows: $M_\infty = 2.5$; $P_{t\infty} = 275{,}790$ Pa (40 psia); and $T_{t\infty} = 294$ K (530°R). Jet conditions were as follows: $d/d_j = 9.4$, $M_j = 2.6$, $P_{tj}/P_{t2} = 12$, and $T_{tj} = T_{t\infty}$. The ratio of the jet momentum ($\rho A V_e^2$) to that of the freestream is approximately 0.5. This is much larger than the 0.1 transition point found by Tolle.[10] However, Tolle's work was done at Mach 14. This means that Tolle's P_{t2} was significantly lower than Finley's (Mach 2.5). From this, coupled with the flow stability, one concludes that all of Finley's regimes are of the blunt-body flow type. This assumption is

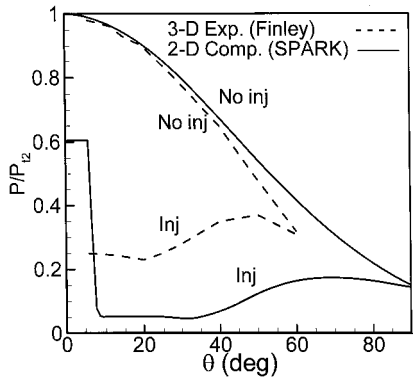

Fig. 2 Comparison of Finley's three-dimensional experimental and current two-dimensional computational results. P_{t2} = 136,942 Pa.

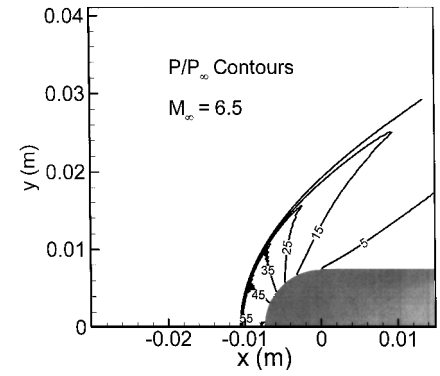

Fig. 3 Nondimensional pressure contours for reference (no-injection) case. P_∞ = 1185.5 Pa.

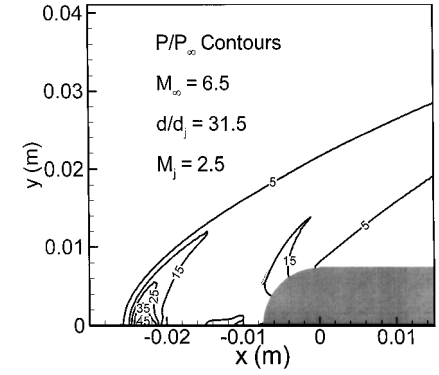

Fig. 4 Nondimensional pressure contours for d/d_j = 31.5 and M_j = 2.5. P_∞ = 1185.5 Pa.

confirmed by schlieren photographs from Ref. 12. Finley found that the blunt-body flow is stable for regimes 1 and 3. Regime 2, which Finley found unstable, occurs over a very small range of P_{tj}/P_{t2} and would have been difficult to observe in the broad studies of Refs. 8 and 9. Results of the test case are shown in Fig. 2, which shows the ratio of static pressure on the body to total pressure after the shock P/P_{t2}, as a function of the angle on the body. Finley's experimental results are shown as dashed lines, whereas the solid lines are the results from the present analysis. The flat region (at approximately $P/P_{t2} = 0.6$, $\theta = 0$) is caused by the jet. At first glance the injection cases do not appear to correlate very well. However, Finley's experiment was done for a three-dimensional sphere-cone, whereas the current results are for a two-dimensional cylinder-wedge geometry. Examination of shock shape and stand-off relations from Billig[13] assists in explaining why the pressures on the surface vary between the experimental (three-dimensional) and computational (two-dimensional) results for the injection case of Fig. 2. Billig developed relations for shock stand-off distance for spherical and cylindrical bodies as

$$\Delta_{\text{sphere}} = (d/2)0.143 \exp\left(3.24/M_\infty^2\right) \tag{3}$$

$$\Delta_{\text{cylinder}} = (d/2)0.386 \exp\left(4.67/M_\infty^2\right) \tag{4}$$

where d is the blunt-body diameter and Δ is measured from the nose tip on the stagnation streamline. Equations (3) and (4) give

$$\frac{\Delta_{\text{cylinder}}}{\Delta_{\text{sphere}}} = 3.393 \qquad \text{at} \quad M_\infty = 2.5 \tag{5}$$

Thus, Δ for a two-dimensional cylinder-wedge will be approximately 3.4 times as large as that for a three-dimensional sphere-cone at $M_\infty = 2.5$ as a result of the relieving effect in the three-dimensional flow. Because the two-dimensional case has a larger Δ, the jet can penetrate further upstream resulting in lower pressures on the body surface. The key aspect of this comparison is that the trends of P/P_{t2} from the present analysis agree well with Finley's results. Subsequent results also agree with trends described in Ref. 12.

Results and Discussion

The effect of upstream injection on the wave drag, heat transfer, and skin-friction drag are investigated for a two-dimensional blunt body with a cylindrical nose, flying at Mach 6.5 with ambient conditions at an altitude of 30 km ($P_\infty = 1185.5$ Pa, $T_\infty = 231.24$ K). A matrix of 15 cases as well as a reference (no-injection) case are studied. Three ratios of d/d_j (63.0, 31.5, and 21.0) are used. At each d/d_j jet exit Mach numbers of 2.0, 2.25, 2.5, 2.75, and 3.0 are considered. Jet exit conditions are calculated from reservoir conditions: $P_{tj} = 375$ kPa and $T_{tj} = 600$ K using standard isentropic flow relations. Thus, given M_j, d_j (equal to area of the jet for two-dimensional problem), P_{tj}, and T_{tj}, all jet exit conditions are readily determined. This method requires that the throat area change for each case in order to meet the required exit conditions.

Reference Case

Figure 3 shows pressure contours for the no-injection case. The shock shape and Δ are shown and agree well with the results of Billig.[13] The centerline stagnation pressure of 55 times the freestream value also agrees closely with standard shock tables. The no-injection, reference values are $\Delta_{\text{ref}} = 0.0030$ m, $D_{\text{ref}} = 295.35$ N/m, $Q_{\text{ref}} = 10{,}083$ W/m, and $F_{\text{ref}} = 5.153$ N/m.

Wave/Jet Drag

Figure 4 shows pressure contours with upstream injection for $d/d_j = 31.5$ and $M_j = 2.5$. For this case the shock standoff distance has approximately increased by six times the no-injection case (i.e., $R_\Delta = 6.10$). This results in significantly lower pressures on the body. The maximum P/P_∞ value is about 20 and occurs near the center of the $P/P_\infty = 15$ contour line on the body. This can also be seen in Fig. 5, which shows P/P_∞ on the nose for $\theta = 0$–90 deg for $d/d_j = 31.5$ and $M_j = 2$, 2.5, and 3. The no-injection curve is also shown for reference. The pressure on the body with injection is generally much less than when there is no injection. Figure 5 shows two key aspects. The first is the large jump in pressure near $\theta = 0$ as a result of the fixed jet exit pressure, which makes a large contribution to the drag, and the second is the peak of the P/P_∞ curve, which is a function of T_j (or M_j). The lower this peak is and the larger the value of θ at which it occurs, the lower the wave drag is because local wave drag is proportional to $P \cos\theta$. Although a P/P_∞ curve may have a very low peak located near 90 deg indicating a reduction in wave drag, the jet exit pressure also contributes to overall wave/jet drag. To move the shock far from the body (pressure peak to large θ), a large jet exit pressure is required. Thus, there is a tradeoff between the height and position of the peak in Fig. 5 and the jet exit pressure. Figure 5 illustrates how these two key aspects of wave/jet drag work together to change the pressure on the body.

Figure 6 shows R_D (drag reduction) as a function of jet Mach number and d/d_j. Recall that R_D accounts for the reverse thrust of the jet as a contribution to the drag. As M_j is increased, there

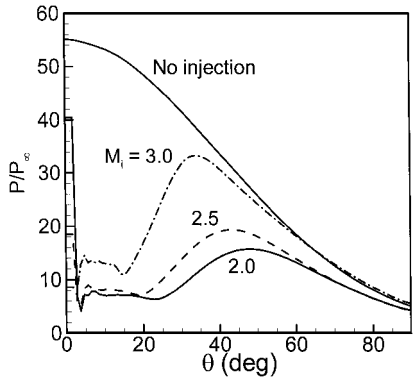

Fig. 5 Nondimensional pressure distribution on blunt-body nose for $d/d_j = 31.5$. $P_\infty = 1185.5$ Pa.

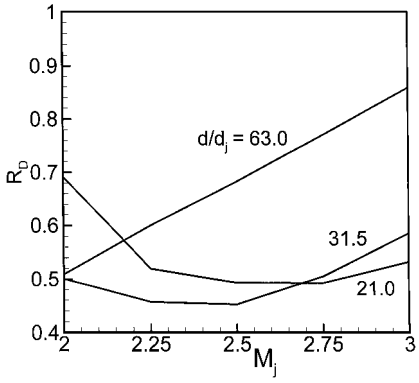

Fig. 6 Drag ratio as a function of jet Mach number. $D_{\text{ref}} = 295.35$ N/m.

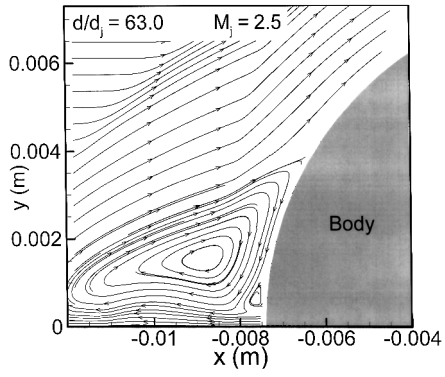

Fig. 7 Close-up view of streamlines showing reattachment point for largest d/d_j, 63.0.

is a bucket in the drag for $d/d_j = 31.5$ and 21.0. A bucket would occur for the $d/d_j = 63.0$ case if one extrapolated the curve to lower M_j. Figure 6 clearly shows that for a given d/d_j and freestream condition there are optimum jet conditions to minimize the drag. If the jet thrust is too small (large M_j), the jet is not being used to its fullest potential to move the shock away from the body. However, if the jet thrust is too large (small M_j), the upstream thrust created by the jet alone will contribute to the overall drag, increasing R_D. The minimum values are as low as 45% of the no-injection case.

There are three main factors that affect the drag: 1) thrust of the jet, 2) Δ, which is affected by the jet thrust, and 3) diameter ratio d/d_j. As shown by Figs. 3 and 4, the larger the Δ, the lower the value of the maximum pressure ratio on the body. To reduce the drag, the reattachment point also must be moved as far aft on the body as possible. Moving the attachment point shifts the peak of the curves in Fig. 5 as discussed earlier. The importance of d/d_j in this respect is now examined. From Fig. 7 it is clear that the center of vorticity is at approximately $y = 0.0016$ m and a reattachment point exists

Table 1 R_D as a function of d/d_j and M_j, $D_{\text{ref}} = 295.35$ N/m

	M_j				
d/d_j	2.00	2.25	2.50	2.75	3.00
63.0	0.509	0.600	0.682	0.770	0.859
31.5	0.501	0.457	0.452	0.505	0.586
21.0	0.691	0.520	0.493	0.493	0.533

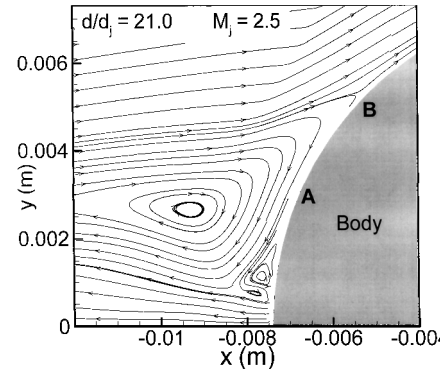

Fig. 8 Close-up view of streamlines showing reattachment point for smallest d/d_j, 21.0.

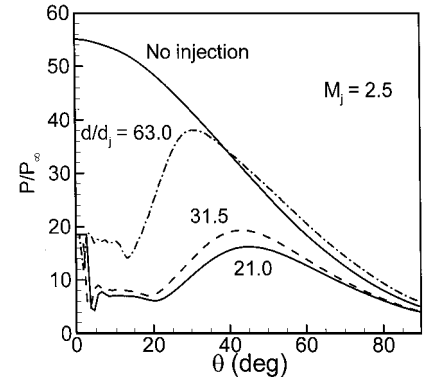

Fig. 9 Nondimensional pressure distribution on blunt-body nose for $M_j = 2.5$. $P_\infty = 1185.5$ Pa.

at $y = 0.0038$ m (or $\theta = 30$ deg). Figure 8 shows the same area on the body at the same M_j with d/d_j one-third that of Fig. 7. The center of vorticity has moved to approximately $y = 0.0026$ m, and the reattachment point is now at $y = 0.0051$ m (or $\theta = 43$ deg). Thus, at smaller d/d_j the reattachment point moves further aft (larger θ on Fig. 1), and therefore the pressure drag component is reduced. Figure 9 clarifies this point. This figure shows P/P_∞ on the body for $M_j = 2.5$ with varying d/d_j. The no-injection case is also shown. The peak of each curve moves to larger values of θ (further aft on the body) as d/d_j is reduced (the height of the peaks are dependent on Δ, which is dependent on C_T). From Figs. 7 and 8 the angles of the reattachment points can be calculated as approximately $\theta = 30$ and 43 deg, respectively. By comparing these values to the same cases on Fig. 9, it is seen that the maximum pressure ratio occurs slightly aft of the reattachment point. Thus, as the reattachment point moves aft on the body, the peak of the curve shifts to larger values of θ, and the wave drag decreases because drag is proportional to $P\cos\theta$. This analysis has examined three main related parameters that control wave/jet drag reductions: d/d_j, Δ, and T_j. The two latter of these parameters are directly dependent on C_T. Careful choice of these three parameters can lead to significant drag reduction as shown in Table 1, which shows R_D as a function of d/d_j and M_j.

Heat-Transfer Rate

The heat-transfer rate is calculated from the stagnation point to the end of the body, $x = 0.015$ m, in order to study the heating/cooling

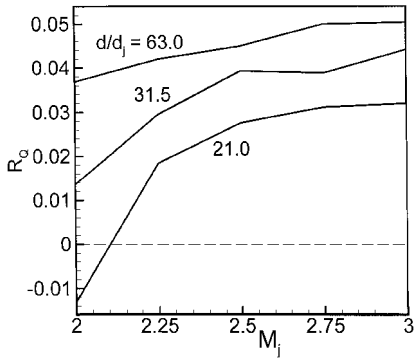

Fig. 10 Heat-transfer rate as a function of jet exit Mach number. Q_{ref} = 10,083 W/m.

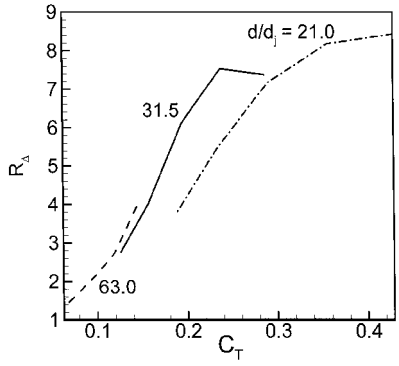

Fig. 11 R_Δ as a function of jet thrust coefficient. Δ_{ref} = 0.0030 m.

effects of forward-facing injection. The main parameters controlling heat transfer to the body are the same as those that control drag. Figure 10 shows R_Q (heat transfer normalized by the reference no-injection heat transfer) as a function of M_j for three values of d/d_j. As the M_j increases for a constant value of d/d_j, Q increases. It must be remembered that the jet total pressure and total temperature are the same for all cases. Thus, as M_j increases, the jet thrust decreases, which decreases Δ. This relationship between jet thrust (or C_T) and Δ (or R_Δ) can be seen in Fig. 11. Note that R_Δ increases as C_T increases. The rate of increase becomes smaller as C_T becomes large, indicating that R_Δ will reach a limiting value for large thrust coefficients. For the cases in this study, an increase in C_T (reduction in M_j) corresponds to an increase in R_Δ (or Δ) for all values of C_T (except for one point as seen in Fig. 11). As the shock moves away from the body, the thickness of the layer of jet air washing over the body increases. Because the fluid is exhausted at relatively cool temperatures, the thicker fluid layer reduces the heat transfer to the body. Figure 12 shows injectant air contours for $M_j = 2$ and 3 at $d/d_j = 31.5$. The air injected at $M_j = 2$ in Fig. 12 is very cool compared to the body. In fact, if the jet penetrates upstream even further, as in the $M_j = 2.0$, $d/d_j = 21.0$ case, the airflow actually cools the flow around the body at 1.30% of the heat-transfer rate for the no-injection case, i.e., $R_Q = -0.0130$ as shown in Fig. 10. For the $M_j = 3$ case in Fig. 12, the body is being heated at a rate of 4.42% of the no-injection case, i.e., $R_Q = 0.0442$ on Fig. 10. When the injected fluid penetrates further upstream (larger Δ), it also expands more as a result of the region of low-pressure air recirculating in the jet near the body seen in Figs. 7 and 8. This expansion creates a thicker boundary layer and thus decreases heating. Figure 13 shows the importance of Δ (which directly affects the fluid thickness over the body). From this figure an inverse relationship between R_Q and R_Δ can be seen. This figure suggests that the major factor in heat transfer to the body is Δ. Table 2 gives numerical values for R_Q as a function of d/d_j and M_j.

Table 2 R_Q as a function of d/d_j and M_j, Q_{ref} = 10,083 W/m

	M_j				
d/d_j	2.00	2.25	2.50	2.75	3.00
63.0	0.0368	0.0420	0.0450	0.0500	0.0504
31.5	0.0136	0.0296	0.0393	0.0388	0.0442
21.0	−0.0130	0.0185	0.0276	0.0312	0.0325

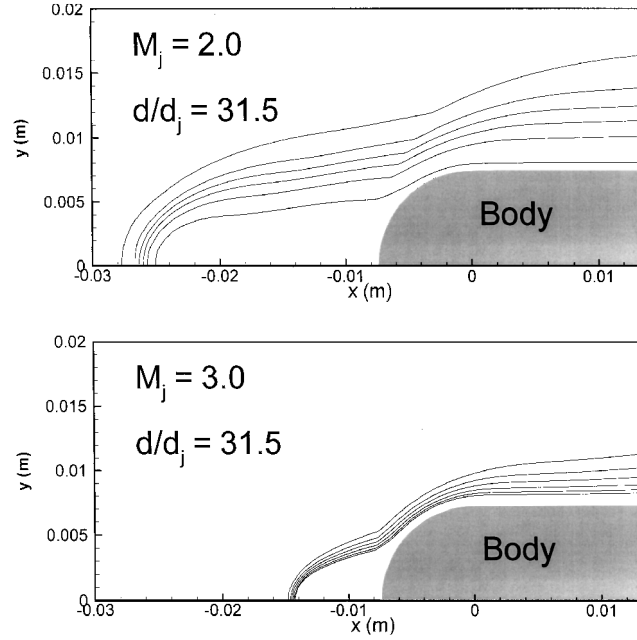

Fig. 12 Jet fluid contours showing injectant thickness over body for jet Mach number of 2.0 and 3.0 with d/d_j = 31.5.

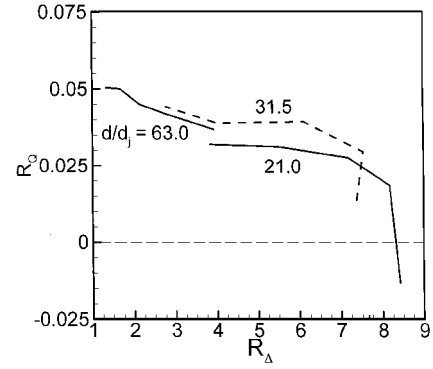

Fig. 13 Heat-transfer rate as a function of shock stand-off ratio. Q_{ref} = 10,083 W/m; Δ_{ref} = 0.0030 m.

Skin-Friction Drag

Leading-edge skin-friction drag is usually dominated by wave drag at hypersonic velocities; however, it is still of interest to see how it is affected as a result of upstream injection. The recirculation zone is largely responsible for skin-friction drag reduction. The recirculation causes the flow to move upstream along the body, which causes a decrease in the total skin-friction drag (Figs. 7 and 8 show the recirculation zone). As the size of the recirculation zone increases, more of the body experiences reverse shear (upstream) as a result of the recirculating fluid. Figure 14 shows this effect clearly. The no-injection case is shown for reference. The local skin-friction drag is nondimensionalized by the value of local skin-friction drag for the no-injection case at $\theta = 90$ deg, $F_{ref}(90)$. Figure 14 shows that as d/d_j decreases (increasing the size of the recirculation region) the bucket in the $F(\theta)/F_{ref}(90)$ curve becomes deeper (more negative) and moves to larger values of θ. This indicates that the reattachment point is moving aft on the body and the size of the recirculation zone is increasing. The bucket in the curves is located on the body near the midpoint between the jet and the reattachment point. This

Table 3 R_F as a function of d/d_j and M_j, F_{ref} = 5.153 N/m

	M_j				
d/d_j	2.00	2.25	2.50	2.75	3.00
63.0	0.396	0.468	0.498	0.509	0.529
31.5	0.280	0.289	0.327	0.389	0.452
21.0	0.262	0.271	0.306	0.348	0.403

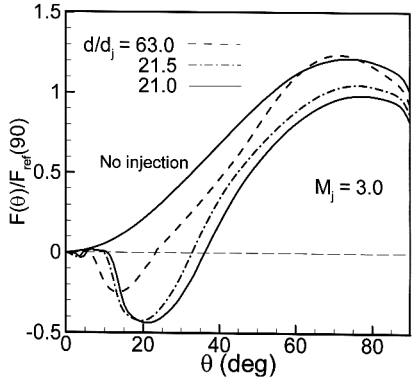

Fig. 14 Nondimensional local skin-friction drag as a function of angle on body nose for M_j = 3.0. $F_{ref}(90)$ = 0.02547 N/m.

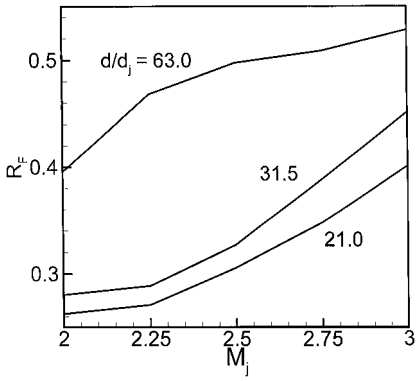

Fig. 15 Nondimensional skin-friction drag as a function of jet Mach number. F_{ref} = 5.153 N/m.

is shown as region A in Fig. 8 and corresponds to where the reverse velocity near the body is highest. From Fig. 14 it can be seen that the local skin-friction drag passes through the $F(\theta)/F_{ref}(90) = 0$ at the reattachment point. This is shown as region B on Fig. 8. As the flow reattaches and begins to move downstream, the skin-friction drag becomes positive. Thus, the larger this recirculation region, the more of a given curve in Fig. 14 will be below the $F(\theta)/F_{ref}(90) = 0$ line, thus resulting in lower total skin-friction drag. If upstream injection is present, a reduction in skin-friction drag is expected because there will always be a recirculation zone. The total skin-friction drag on the nose F_N can be calculated using the data from Fig. 14. Because Fig. 14 presents the local skin-friction drag as a function of the angle on the body, the drag on the nose of the body caused by skin friction can be calculated from Eq. (6):

$$F_N = F_{ref}(90) \int_0^{90} \frac{F(\theta)}{F_{ref}(90)}\, d\theta \tag{6}$$

By including the skin friction from $x = 0$ to 0.015 in Eq. (6) (which is $\theta > 90$ deg, not shown in Fig. 14), the total skin-friction drag F may be found. Figure 15 shows the skin-friction drag as a function of M_j for specific values of d/d_j. As just stated, smaller values of d/d_j yield lower values of R_F. For a given d/d_j the skin-friction drag increases as M_j increases. This occurs because the jet thrust is decreasing, decreasing Δ, which decreases the size of the recirculation region, moving the reattachment point to smaller θ, which causes an increase in the total skin-friction drag. Table 3 gives numerical values for R_F as a function of d/d_j and M_j.

Conclusions

The effects of a supersonic jet injecting upstream from the stagnation point of a blunt body flying at Mach 6.5 at 30 km altitude are investigated. Specifically, wave drag, heat transfer, and skin-friction drag on the leading edge of the body are examined. The injection is shown to significantly modify the flowfield. Wave drag including the drag penalty of the forward-facing jet is shown to reduce by as much as 55%. Heat-transfer rates can be dramatically reduced and can actually reverse, i.e., the flow along the body surface cools the flow around the body in the leading-edge region. Skin-friction drag is also shown to decrease as a result of upstream injection. The primary mechanisms controlling wave drag and skin-friction drag are found to be shock stand-off distance and the ratio of body diameter to jet diameter. The heat-transfer rate is governed primarily by the shock stand-off distance. By using proper jet exit conditions, the wave drag, heat-transfer rate, and skin-friction drag can be significantly reduced. Larger blunt-body noses, which allow for the inclusion of injectors, can use forward jet(s) to reduce and even eliminate thermal loads while simultaneously reducing the drag of hypersonic leading edges.

Appendix A: Convergence

An intensive grid- and time-convergence study was undertaken. Three grids were used for both the injection and no-injection case. Each successive grid increased the number of points in the boundary layer at least two fold. For time convergence the number of iterations was increased by increments of 75,000 until steady state was reached. Table A1 shows the time convergence by the percent change of wave drag, heat transfer, and skin-friction drag over the final 75,000 iterations. In the case of injection, this is the percent change between 300,000 and 375,000 iterations. When the solutions from all three grids reached steady-state convergence, they were compared to each other for grid convergence. Table A1 shows grid convergence by the percent change in wave drag, heat transfer, and skin-friction drag between the time converged second and third grids (refined and most refined grids). All values are converged to at least 10%, with most converging to at least 5%. The refined grid was used in the calculations for injection. It contained 145 × 97 points in the tangential and radial directions. The run time for solutions using this grid were on the order of 36 h on a HP-9000/782 workstation.

Appendix B: Thrust and Mach Relationship

This section shows the inverse relationship between jet Mach number and jet thrust with constant total pressure and temperature and with constant jet exit area (note that throat area changes to meet required conditions). The first step is to write the equation for thrust:

$$T_j = \dot{m} V_e + A_e P_e \tag{B1}$$

Equation (B1) can be rewritten as

$$T_j = A_e P_e \left(\gamma M_j^2 + 1\right) \tag{B2}$$

with $\gamma = 1.4$. Differentiating Eq. (B2) with respect to M_j yields

$$\frac{\partial T_j}{\partial M_j} = A_e P_e (2\gamma M_j) + A_e \left(\gamma M_j^2 + 1\right) \frac{\partial P_e}{\partial M_j} \tag{B3}$$

Table A1 Grid and time convergence

	Injection		No injection	
	Time, %	Grid, %	Time, %	Grid, %
Wave drag	0.25	2.12	0.00	0.00
Heat transfer	1.56	5.97	0.02	9.75
Skin friction	0.99	10.4	0.02	4.24

By differentiating the following equation for P_{tj} (constant) with respect to M_j

$$P_{tj} = P_e\left\{1 + [(\gamma - 1)/2]M_j^2\right\}^{\gamma/(\gamma-1)} \tag{B4}$$

one can solve for $\partial P_e/\partial M_j$ and obtain

$$\frac{\partial P_e}{\partial M_j} = \frac{-\gamma P_e M_j}{1 + [(\gamma - 1)/2]M_j^2} \tag{B5}$$

Equation (B5) can then be substituted into Eq. (B3) to obtain

$$\frac{\partial T_j}{\partial M_j} = 2\gamma A_e M_j P_e\left[\frac{1 - M_j^2}{2 + (\gamma - 1)M_j^2}\right] \tag{B6}$$

All of the variables in Eq. (B6) are positive. Thus, from the numerator term in the parentheses, if M_j is greater than one (which is always the case for this study), the change in thrust with respect to jet Mach number will be negative. Therefore, as the jet Mach number increases, the jet thrust will decrease. This can also be seen by solving Eq. (B4) for P_e and substituting into Eq. (B2) to obtain

$$T_j = A_e P_{tj}\frac{\left(\gamma M_j^2 + 1\right)}{\left\{1 + [(\gamma - 1)/2]M_j^2\right\}^{\gamma/(\gamma-1)}} \tag{B7}$$

Because A_e and P_{tj} are constant, one sees from Eq. (B7) that the denominator will dominate as M_j is increased, decreasing T_j. Figure B1 shows the relationship between the thrust and Mach number of the jet. As shown by Eqs. (B6) and (B7), as the jet Mach number increases, the jet thrust decreases. The different slopes in the curves are caused by the different exit areas. From Eq. (B4) one notes that with γ and P_{tj} constant P_e will have the same value for all curves in Fig. B1 for a given M_j. For given P_e, M_j, and γ, the slopes of the curves $\partial T_j/\partial M_j$ are governed by A_e as shown by Eq. (B6). As A_e increases, d/d_j decreases. Thus, for the smallest d/d_j, $\partial T_j/\partial M_j$ has the largest negative value.

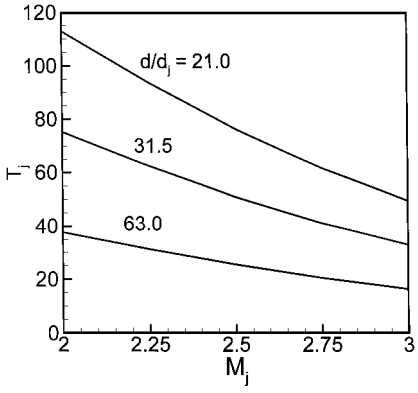

Fig. B1 Jet thrust as a function of jet Mach number.

Acknowledgments

This research has been partially funded by NASA NAG-1-2167 Grant from the HYPER-X Program Office, C. R. McClinton, Technical Monitor, NASA Langley Research Center, Hampton, Virginia.

References

[1]Hutt, C. R., and Howe, A. J., "Forward Facing Spike Effects of Bodies of Different Cross Section in Supersonic Flow," *The Aeronautical Journal of the Royal Aeronautical Society*, Vol. 93, No. 6, 1989, pp. 229–234.

[2]Yamauchi, M., Fujii, K., and Higashino, F., "Numerical Investigation of Supersonic Flows Around a Spiked Blunt Body," *Journal of Spacecraft and Rockets*, Vol. 32, No. 1, 1995, pp. 32–42.

[3]Riggins, D. W., Nelson, H. F., and Johnson, E., "Blunt Body Wave Drag Reduction Using Focused Energy Deposition," *AIAA Journal*, Vol. 37, No. 4, 1998, pp. 460–504.

[4]Toro, P. G. P., Nagamatsu, H. T., Minucci, M. A. S., and Myrabo, L. N., "Experimental Pressure Investigation of a 'Directed-Energy Air Spike' Inlet at Mach 10," AIAA Paper 99-2843, June 1999.

[5]Toro, P. G. P., Nagamatsu, H. T., Myrabo, L. N., and Minucci, M. A. S., "Experimental Heat Transfer Investigation of a 'Directed-Energy Air Spike' Inlet at Mach 10," AIAA Paper 99-2844, June 1999.

[6]Matsuo, A., Fujii, K., and Fujiwara, T., "Flow Features of Shock-Induced Combustion Around Projectile Traveling at Hypervelocities," *AIAA Journal*, Vol. 33, No. 6, 1995, pp. 1056–1063.

[7]Charczenko, N., and Hennessey, K. W., "Investigation of a Retrorocket Exhausting from the Nose of a Blunt Body into a Supersonic Free Stream," NASA TN D-751, Sept. 1961.

[8]Love, E. S., "The Effects of a Small Jet of Air Exhausting from the Nose of a Body of Revolution in Supersonic Flow," NACA RM L52I19a, 12 Nov. 1952.

[9]Romeo, D. J., and Sterrett, J. R., "Exploratory Investigation of the Effect of a Forward-Facing Jet on the Bow Shock of a Blunt Body in a Mach 6 Free Stream," NASA TN D-1605, Feb. 1963.

[10]Tolle, F. F., "An Investigation of the Influence of a Forward Ejected Gas Stream on Hypersonic Flow About Blunt Bodies," Ph.D. Dissertation, Dept. of Aerospace and Mechanical Engineering, Univ. of Arizona, Tucson, AZ, 1973.

[11]Drummond, J. P., Rogers, R. C., and Hussaini, M. Y., "A Detailed Numerical Model of a Supersonic Mixing Layer," AIAA Paper 86-1427, June 1986.

[12]Finley, J. P., "The Flow of a Jet from a Body Opposing a Supersonic Free Stream," *Journal of Fluid Mechanics*, Vol. 26, Pt. 2, Oct. 1966, pp. 337–368.

[13]Billig, F. S., "Shock Wave Shapes Around Spherical- and Cylindrical-Nosed Bodies," *Journal of Spacecraft and Rockets*, Vol. 4, No. 6, 1967, pp. 822, 823.